



POTSDAM-INSTITUT FÜR
KLIMAFOLGENFORSCHUNG







Originally published as:

Tagne Nkouna, I., [Marwan, N.](#), Moukam Kakmeni, F., Yamapi, R., [Kurths, J.](#) (2023): Adaptive resonance and control of chaos in a new memristive generalized FitzHugh-Nagumo bursting model. - Chaos, 33, 10, 103106.

DOI: <https://doi.org/10.1063/5.0166691>

RESEARCH ARTICLE | OCTOBER 02 2023

Adaptive resonance and control of chaos in a new memristive generalized FitzHugh-Nagumo bursting model

I. B. Tagne Nkouna  ; N. Marwan ; F. M. Moukam Kakmeni ; R. Yamapi ; Jürgen Kurths 



Chaos 33, 103106 (2023)

<https://doi.org/10.1063/5.0166691>



View
Online



Export
Citation

CrossMark



APL Quantum
Bridging fundamental quantum research with technological applications

Now Open for Submissions
No Article Processing Charges (APCs) through 2024

Submit Today



Adaptive resonance and control of chaos in a new memristive generalized FitzHugh-Nagumo bursting model

Cite as: Chaos 33, 103106 (2023); doi: 10.1063/5.0166691

Submitted: 6 July 2023 · Accepted: 8 September 2023 ·

Published Online: 2 October 2023



View Online



Export Citation



CrossMark

I. B. Tagne Nkouna,^{1,a)} N. Marwan,² F. M. Moukam Kakmeni,³ R. Yamapi,¹ and Jürgen Kurths^{2,4}

AFFILIATIONS

¹Fundamental Physics Laboratory, Physics of Complex System Group, Department of Physics, Faculty of Science, University of Douala, Box 24 157 Douala, Cameroon

²Potsdam Institute for Climate Impact Research (PIK), Member of the Leibniz Association, Telegraphenberg, P.O. Box 601203, 14473 Potsdam, Germany

³Complex Systems and Theoretical Biology Group and Laboratory of Research on Advanced Materials and Non-linear Science (LaRAMaNS), Department of Physics, Faculty of Science, University of Buea, P.O. Box 63, Buea, Cameroon

⁴Department of Physics, Humboldt University, 12489 Berlin, Germany

^{a)} Author to whom correspondence should be addressed: boristagne060@gmail.com

ABSTRACT

In a new memristive generalized FitzHugh–Nagumo bursting model, adaptive resonance (AR), in which the neuron system's response to a varied stimulus can be improved by the ideal intensity of adaptation currents, is examined. We discovered that, in the absence of electromagnetic induction, there is signal detection at the greatest resonance peak of AR using the harmonic balance approach. For electromagnetic induction's minor impacts, this peak of the AR is optimized, whereas for its larger effects, it disappears. We demonstrate dependency on adaption strength as a bifurcation parameter, the presence of period-doubling, and chaotic motion regulated and even annihilated by the increase in electromagnetic induction using bifurcation diagrams and Lyapunov exponents at specific resonance frequencies. The suggested system shows the propagation of localized excitations as chaotic or periodic modulated wave packets that resemble breathing structures. By using a quantitative recurrence-based analysis, it is possible to examine these plausible dynamics in the structures of the recurrence plot beyond the time series and phase portraits. Analytical and numerical analyses are qualitatively consistent.

Published under an exclusive license by AIP Publishing. <https://doi.org/10.1063/5.0166691>

In general, the non-permissive (silence or subthreshold) and permissive (nerve pulse) states are typical regimes characterizing neuron dynamics. A generalized FitzHugh–Nagumo neural system with tristable activity instead of the computationally intensive, high-dimensional Hodgkin-Huxley type model has been recently built and suggested to explain three states of neurons depending on the state of ionic conductance (initial conditions). Electrical signals of spiking, periodic and chaotic bursting, and breather dynamics have been well reproduced by biological neurons containing adaption currents, and the effects of electromagnetic induction (EMI) on those dynamics have been well studied. The hidden information of those dynamics is usually revealed using the method of recurrence analysis. Signal detection by stochastic resonance (SR) and even vibration resonance (VR) is the important result well found in neural systems. Based on that simple tristable neural system coupled to internal effects such as

adaption currents and EMI, we respond in this paper to signal detection appearing by adaptive resonance (AR) through adaption strength, breathing structures, and the control of adaptive resonance and chaos by electromagnetic induction effects.

I. INTRODUCTION

Stochastic resonance (SR) is an interesting and well-known phenomenon that has attracted considerable attention.^{1–4} This phenomenon, interpreted as noise-enhanced signal detection, explains how the signal-to-noise ratio of the output signal is maximized at an optimum intensity of noise added simultaneously with a weak periodic signal in many systems. In neural systems, SR is marked by the fact that neurons can use stochastic environmental influences to process the input signals.⁴ On the other hand, resonance

dynamics due to a biharmonic external force with two different frequencies where one is smaller than the other has also received much interest.^{5–7} In fact, signal detection in a single neuron and network could also be improved by an optimal amplitude of the high-frequency signal. The later is known in many systems as the vibration resonance (VR) phenomenon.

The recurrence plot (RP) is a visual tool that shows the recurrence patterns in a dynamical system. It has been introduced by Eckmann *et al.*^{8,9} with the aim of having another representation of the dynamics of systems instead of time series and phase portraits. A recurrence is defined as the return of the trajectory of a system to an earlier state. It consists of the graphical representation of a binary symmetric square matrix that encodes the times when two states are in close proximity or simply neighbors in phase space. A large and diverse amount of hidden information on the dynamics of a system can be extracted and statistically quantified using a quantitative description called recurrence quantification analysis (RQA). It has been successfully applied to many fields, including neuroscience.^{10–13}

Electromagnetic induction (EMI) was modeled and its effects broadly studied on neuron dynamics.^{5,14–18} To name a few effects of EMI, it has been found that EMI decreases the bursting firing in the Hindmarsh–Rose (HR) neuron,¹⁹ switches the firing dynamics of the Moris–Lecar (ML) neuron from spontaneous or bursting firing into silent mode,²⁰ suppresses the propagation and breakup of the target wave,²¹ switches the neuron from active to non-active states in a birhythmic conductance-based neuronal model,¹⁴ and optimizes and decreases the peak of VR in the Hodgkin–Huxley (HH) model.⁵ On the other hand, adaption currents have been found to make biological neurons by creating intrinsic periodic and chaotic bursting adapting neurons under a constant external current.²² It has shown the same phenomenon of periodic and chaotic bursting, including the switching of the neural activities from non-active to active states, in a birhythmic conductance-based neuronal model.²³

The new generalized Fitzhugh–Nagumo model is a simple conductance-based model having tristability,²⁴ absent in simple models like HR,²⁵ Fitzhugh–Nagumo FHN,²⁶ and in birhythmic conductance-based neuronal²³ models, and it offers room for analytical analysis difficult to treat in conductance-based models like HH²⁷ and ML²⁸ models. Although the signal detection by SR and VR is well studied in neural systems, an intrinsic detection by adaptive resonance (AR) due to the optimal strength of adaption currents and the appearance of modulated waves-like breathers has to be investigated. Moreover, although EMI effects are well studied on reduced models such as HR, FHN, and Izhikevich neuron models, their effects on AR are yet to be investigated in the new generalized Fitzhugh–Nagumo model.

With this motivation, we propose in this work an extension of a new generalized FHN model coupled to the internal effects of adaptation and electromagnetic induction. Using analytical and numerical analyses of the two-dimensional model without considering those internal effects, we determine the parameter regions where monostable and multistable dynamics are observed. We also analyze the interaction between external sinusoidal stimulus, adaptation currents, and EMI, leading to asymptotic dynamics and recurrence-based analysis. As the results of these studies show, signal detection by adaptive resonance (AR), period-doubling, and chaos controlled and optimized by electromagnetic strength are found. Furthermore,

the structures of the recurrence plot of modulated wave packets-like breathers-type excitations due to the presence of period-doubling and chaos are also shown.

The work is structured as follows: In Sec. II, we present the new two-dimensional neuronal model as an extension of the FHN model motivated by Taylor approximation of the ML model. We then present the four-dimensional model, taking into account adaptation and electromagnetic induction. In Sec. III, we explore the two-dimensional deterministic model. A deterministic bifurcation diagram in one dimension is obtained using Lindsted's perturbation method²⁹ and numerical bifurcation. Then, we explore the effects of adaptation and electromagnetic induction using the harmonic balance method³⁰ and the asymptotic dynamic using bifurcations and the Lyapunov exponent. In Sec. IV, we present typical neuron breathing patterns under the varying strength of adaptation and their corresponding recurrence features obtained by the RP analysis.⁹ In Sec. V, we summarize our work.

II. A MEMRISTIVE GENERALIZED FITZHUGH–NAGUMO BURSTING MODEL

The recent and new generalized FHN neuronal model motivated by the original FHN model²⁶ and the biophysical ML model²⁸ and proposed by some of the authors²⁴ (the details are given in Appendix A) is an extended system expressed in the following form:

$$\begin{aligned} \frac{dv}{dt} &= \alpha_0 v + \alpha_1 v^3 - \alpha_2 v^5 + \alpha_3 v^7 - \alpha_4 v^9 + y + I_{ext}, \\ \frac{dy}{dt} &= \epsilon (1 - cv - 5v^2 - y), \end{aligned} \quad (1)$$

where higher-order terms are additionally included as $\alpha_0 v + \alpha_1 v^3 - \alpha_2 v^5 + \alpha_3 v^7 - \alpha_4 v^9$ containing only odd terms to keep odd symmetry of the function as in the original FHN model.²⁶ The system (1) consists of a nonlinear membrane potential v equation coupled with a recovery variable y of slow ionic currents quadratic equation. The parameters $\alpha_0, \alpha_1, \alpha_2, \alpha_3,$ and α_4 , which are defined as the maximum conductance coefficients of ion channels, constitute the nonlinear function characterizing the transmembrane current changes due to the exchange between the intracellular and extracellular medium of the nerve membrane. The essential characteristics of the system dynamics depend strongly on the choice of these parameters. The conductance coefficients of ion channels $\alpha_1, \alpha_2, \alpha_3,$ and α_4 were set as $\alpha_1 = 2.7778, \alpha_2 = 2.3333, \alpha_3 = 0.7619,$ and $\alpha_4 = 0.0847;$ ²⁴ ϵ and c represent, respectively, small and control parameters in the equation for the recovery variable y .

Mostly in the neuron, slow processes are realized by a gating variable of adaptive currents.^{22,23} Moreover, fluctuations in membrane potential or the transport of ions across the neuronal membrane induce a change in the electromagnetic field.³¹ Therefore, the coupling between a magnetic field and the membrane potential of the neuron is modeled through a memristor.^{14,15,32} Based on the neuron model expressed in Eq. (1), we introduce slow processes such as an adaptation variable and a variable for the magnetic flow in the forms as used in Refs. 15 and 14. A new memristive generalized Fitzhugh–Nagumo bursting neuron model, which will be used in this analysis and designed to describe simultaneous effects of electromagnetic induction and adaption currents on the neuronal

activities, is expressed by the following system:

$$\begin{aligned} \frac{dv}{dt} &= \alpha_0 v + \alpha_1 v^3 - \alpha_2 v^5 + \alpha_3 v^7 - \alpha_4 v^9 + w - \alpha z - k\rho(\phi)v + I_{ext}, \\ \frac{dy}{dt} &= \epsilon(1 - cv - 5v^2 - y), \\ \frac{dz}{dt} &= r(sv - z), \\ \frac{d\phi}{dt} &= k_1 v - k_2 \phi, \\ \frac{dq(\phi)}{dt} &= \rho(\phi) = a + 3b\phi^2. \end{aligned} \tag{2}$$

The third variable, z , describes the adaptation currents; α is the strength feedback; r and s are other positive parameters. The fourth variable, ϕ , describes the magnetic flux across the membrane. The memory conductance of a magnetic flux-controlled memristor³¹ $\rho(\phi)$ materializes the coupling between the magnetic flux and membrane potential of the neuron. The term $\rho(\phi)$ often takes the form of a positive function $\rho(\phi) = a + 3b\phi^2$ where a and b are positive constants. According to Faraday’s law of electromagnetic induction and description of the memristor, $k\rho(\phi)v$ imposes an induction current on neuron.³¹ The membrane potential-induced change in magnet flux and leakage of the magnet flux stand, respectively, for $k_1 v$ and $k_2 \phi$. The parameter k stands for the strength of the feedback current on the membrane potential. The parameters for the memory function and the coefficients that rule the magnetic flux dynamics are given by $a = 0.1$, $b = 0.06$, and $k_1 = 0.1$, $k_2 = 0.5$, respectively.³³ The other parameters have the same meaning and value as the upper ones.

III. DYNAMICS OF THE DETERMINISTIC NEURON MODEL

A. Neural rythms in a generalized Fitzhugh–Nagumo model

An approximation of the amplitudes and frequencies of oscillatory states is obtained first by reducing our two-dimensional coupled system (1) without considering internal effects ($\alpha = k = 0$) to a second-order scalar equation and second by eliminating the y variable and setting $t = \Omega_0 \tau$. The following equation like the dimensionless model in the Lienard form³⁴ is expressed as follows:

$$\begin{aligned} \ddot{v} - \mu(-\gamma_0 + \gamma_1 v^2 - \gamma_2 v^4 + \gamma_3 v^6 - \gamma_4 v^8) \dot{v} + v \\ = \epsilon \mu^2 \left(-1 - 5v^2 + \frac{1}{3} \gamma_1 v^3 - \frac{1}{5} \gamma_2 v^5 + \frac{1}{7} \gamma_3 v^7 - \frac{1}{9} \gamma_4 v^9 \right) + E_{ext}, \end{aligned} \tag{3}$$

where

$$\begin{aligned} \mu &= \frac{1}{\Omega_0}, & \gamma_1 &= 3\alpha_1, & \gamma_2 &= 5\alpha_2, & \gamma_3 &= 7\alpha_3, & \gamma_4 &= 9\alpha_4, \\ \Omega_0 &= \sqrt{\epsilon(c - \alpha_0)}, & \gamma_0 &= \epsilon - \alpha_0, & E_{ext} &= \frac{\epsilon}{\Omega_0^2} I \left(\frac{t}{\Omega_0} \right), \end{aligned}$$

and the dot denotes the derivative with respect to τ .

Equation (3) has been found and well solved by some of the authors in Ref. 24, using Lindsted’s perturbation method,²⁹ and the solution is approximated as follows:

$$\begin{aligned} v(\tau') &= A \cos \omega \tau' + \mu(\theta_2 \sin \omega \tau' + \theta_3 \sin 3\omega \tau' + \theta_4 \sin 5\omega \tau' \\ &+ \theta_5 \sin 7\omega \tau' + \theta_6 \sin 9\omega \tau') + O(\mu^2), \end{aligned} \tag{4}$$

where the maximum of the membrane potential amplitude A satisfies the following equation:

$$\gamma_0 - \frac{1}{4} \gamma_1 A^2 + \frac{1}{8} \gamma_2 A^4 - \frac{5}{64} \gamma_3 A^6 + \frac{7}{128} \gamma_4 A^8 = 0, \tag{5}$$

and the frequency ω is given by

$$\begin{aligned} \omega &= 1 + \mu^2 \left(\frac{211}{262144} \gamma_4^2 A^{16} - \frac{285}{131072} \gamma_3 \gamma_4 A^{14} \right. \\ &+ \left(\frac{93}{65536} \gamma_3^2 + \frac{69}{20480} \gamma_2 \gamma_4 \right) A^{12} \\ &- \left(\frac{69}{16384} \gamma_2 \gamma_3 + \frac{281}{40960} \gamma_1 \gamma_4 \right) A^{10} \\ &+ \left(\frac{79}{2560} \gamma_0 \gamma_4 + \frac{67}{8192} \gamma_1 \gamma_4 + \frac{3}{1024} \gamma_2^2 \right) A^8 \\ &- \left(\frac{73}{2048} \gamma_0 \gamma_3 + \frac{1}{96} \gamma_1 \gamma_2 + \frac{5}{128} \gamma_3 \right) A^6 \\ &+ \left(\frac{1}{24} \gamma_0 \gamma_2 + \frac{1}{128} \gamma_1^2 + \frac{1}{16} \gamma_2 \right) A^4 \\ &\left. - \left(\frac{3}{64} \gamma_0 \gamma_1 + \frac{1}{8} \gamma_1 \right) A^2 \right) + O(\mu^3). \end{aligned} \tag{6}$$

The steps of the method and unknown parameters of Eq. (4) are given in Appendix B.

The membrane potential amplitude A for different values of the parameter α_0 (Fig. 1) is obtained by the computation of the analytical equation (5) (dark solid line) and the system [Eq. (1)] (red dotted line), through the Newton–Raphson schemes and the fourth-order Runge–Kutta algorithm, respectively. It exhibits the bifurcation curve of the maximum membrane potential vs the conductance parameter α_0 as the bifurcation parameter. However, the higher nonlinear amplitude equation (5) can, depending on the parameters $\alpha_0, \alpha_1, \alpha_2, \alpha_3, \alpha_4$, give four different real positive roots explaining the different levels of the membrane potential of neurons for the same parameter values. These various levels of excitability explain the sensitivity of the neuron to initial conditions (states of ionic conductance) and are important to define its dynamical properties. The model in Eq. (1) exhibits four types of particular regions of existence and coexistence states depending on the range values of the conductance parameter α_0 , and each defining a type of excitability of the neuron, see Table I. The unstable states represent thresholds separating coexisting stable states of the system. Monostability, bistability, tristability, and other behaviors are some characteristics found by this study in the

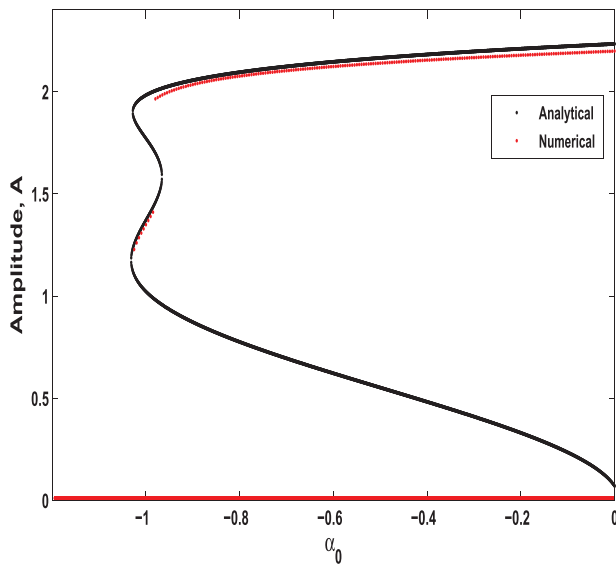


FIG. 1. Analytical (dark solid line) and numerical (red dotted line) bifurcation diagram in the (amplitude, α_0) plane, obtained through Eq. (5). The parameters used are as follows: $\alpha_1 = 2.7778$, $\alpha_2 = 2.3333$, $\alpha_3 = 0.7619$, $\alpha_4 = 0.0847$, $c = 100.0$, $\epsilon = 0.01$, $k = 0.0$, $\alpha = 0.0$, and $l = 0.0$.

neural dynamics like in some biophysical models^{35,36} and are relevant for understanding initiation and information processing in neurons.

B. Signal detection by adaptive resonance and control of chaos

Let us consider the model used to study the dynamic of our neuronal system represented by Eq. (2), taking into account the coupling between simultaneous adaption currents, magnetic field, and membrane potential with, respectively, the strength feedback α and k taken at the non-zero case. Thus, our focus is mainly on the simultaneous effects of the negative feedback strength k and the strength α on the autonomous neuronal dynamic study above in the absence of adaptive currents and EMI. To make this possible, we reduce the system described in Eq. (2) by eliminating the y variable, and we obtain the following system:

$$\begin{cases} \ddot{v} - \mu(-\gamma_0 + \gamma_1 v^2 - \gamma_2 v^4 + \gamma_3 v^6 - \gamma_4 v^8 - k(a + 3b\phi^2)) \dot{v} \\ + v = -\mu(\alpha \dot{z} + 6kb\phi \dot{\phi} v) + \epsilon \mu^2 \left(1 - 5v^2 + \frac{1}{3}\gamma_1 v^3 - \frac{1}{5}\gamma_2 v^6 \right. \\ \left. + \frac{1}{7}\gamma_3 v^7 - \frac{1}{9}\gamma_4 v^9 - \alpha z - k(a + 3b\phi^2)v \right) + I_{ext}, \\ \dot{z} = R(sv - z), \\ \dot{\phi} = q_1 v - q_2 \phi, \end{cases} \quad (7)$$

where

$$\begin{aligned} \mu &= \frac{1}{\Omega_0}, \quad \gamma_1 = 3\alpha_1, \quad \gamma_2 = 5\alpha_2, \quad \gamma_3 = 7\alpha_3, \quad \gamma_4 = 9\alpha_4, \\ \Omega_0 &= \sqrt{\epsilon(c - \alpha_0)}, \quad \gamma_0 = \epsilon - \alpha_0, \quad R = \mu r, \\ q_1 &= \mu k_1, \quad q_2 = \mu k_2, \quad I(t) = \frac{1}{\omega^2} I\left(\frac{t}{\omega_{eff}}\right) = I_{ext}. \end{aligned}$$

Considering an external stimulus with a sinusoidal term $I_{ext} = E \cos \Omega t$ induces a change in the amplitude of the forced membrane potential states. The harmonic balance method³⁰ can be employed to determine this amplitude. By considering the frequency of the fundamental component of the solutions as the same as the stimulus, the evolution of the membrane potential v is given as follows:

$$v(t) = A_1 \cos \Omega t + A_2 \sin \Omega t = A_c \cos(\Omega t - \psi). \quad (8)$$

By substituting Eq. (8) into Eq. (7), we obtain a particular solution of the variables ϕ and z as follows:

$$\phi(t) = (\eta_1 A_1 - \Omega \eta_2 A_2) \cos \Omega t + (\eta_1 A_2 + \Omega \eta_2 A_1) \sin \Omega t, \quad (9)$$

$$z(t) = (\Gamma_1 A_1 - \Omega \Gamma_2 A_2) \cos \Omega t + (\Gamma_1 A_2 + \Omega \Gamma_2 A_1) \sin \Omega t, \quad (10)$$

where

$$\begin{aligned} \eta_1 &= \frac{q_1 q_2}{q_2^2 + \Omega^2}, \quad \eta_2 = \frac{1}{q_2} \eta_1, \\ \Gamma_1 &= \frac{R^2 s}{R^2 + \Omega^2}, \quad \Gamma_2 = \frac{1}{R} \Gamma_1. \end{aligned}$$

Inserting Eqs. (8)–(10) into Eq. (7) and equating the coefficient of cosine and sine terms separately, the amplitude of the oscillatory states satisfies the following algebraic equation:

$$\begin{aligned} F_1 A_c^{18} + F_2 A_c^{16} + F_3 A_c^{14} + F_4 A_c^{12} + F_5 A_c^{10} + F_6 A_c^8 + F_7 A_c^6 \\ + F_8 A_c^4 + F_9 A_c^2, \end{aligned} \quad (11)$$

where

$$\begin{aligned} A_c^2 &= A_1^2 + A_2^2, \\ \tan \psi &= \mu \Omega \frac{\left(\gamma_0 - \frac{1}{4}\gamma_1 A_c^2 + \frac{1}{8}\gamma_2 A_c^4 - \frac{5}{64}\gamma_3 A_c^6 + \frac{7}{128}\gamma_4 A_c^8 + Q \right)}{(1 - \Omega^2 + P)}, \end{aligned}$$

TABLE I. Table summarizing the stability, the dynamical behavior of different parameter regions, and the corresponding neuron types.²⁴

Values of α_0	Stability	Behavior	Neuron type
$[-1.200, -1.029[$	Monostable	Quiescent state	Integrator with the excitability of class I
$[-1.029, -1.016[$	Bistable	Quiescent state subthreshold oscillation	Resonator with the excitability of class I
$[-1.016, -0.968]$	Tristable	Quiescent state subthreshold oscillation	Resonator with the excitability of class II
$] -0.968, 0.009]$	Bistable	large-amplitude oscillation Quiescent state large-amplitude oscillation	Resonator with the excitability of class II

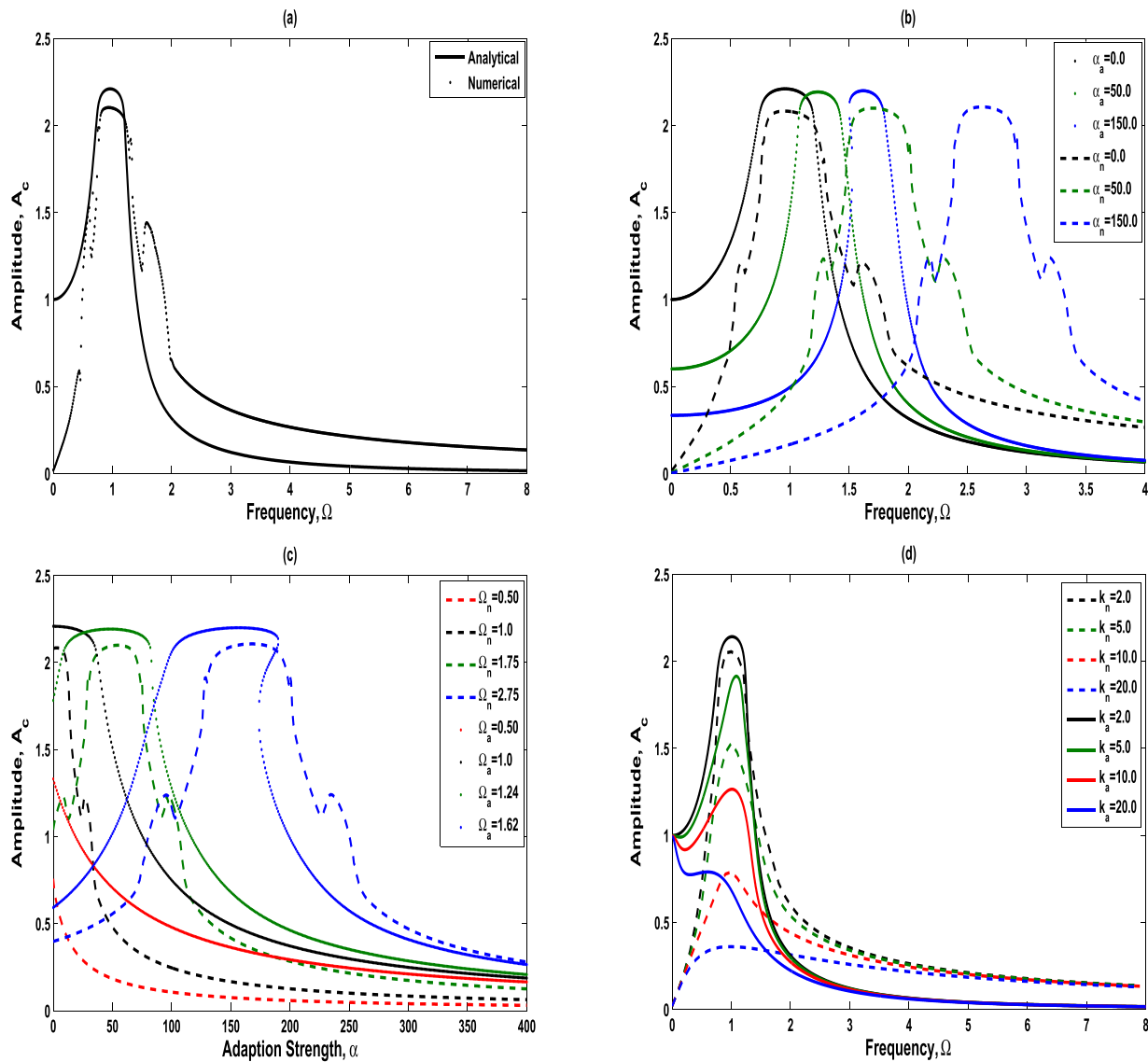


FIG. 2. Comparison between analytical (dark line) and numerical (dark dots) frequency-response curves for $k = \alpha = 0.0$ (a). Analytical (lines) and numerical (dots) frequency-response curves for different values of α (b) and k (d). Analytical (lines) and numerical (dots) curves of amplitude vs α for different values of Ω (c), $k = 0.0$. Ω_n and Ω_a are, respectively, the numerical and analytical frequency; α_n and α_a are, respectively, the numerical and analytical adaption strength; while k_n and k_a are, respectively, the numerical and analytical EMI strength k . The parameters used are as follows: $l = 1.0, k_1 = 0.1, k_2 = 0.5, a = 0.1, b = 0.06, r = 0.01, s = 4.0, \alpha_0 = -1.1, \alpha_1 = 2.7778, \alpha_2 = 2.3333, \alpha_3 = 0.7619, \alpha_4 = 0.0847, c = 100.0$, and $\epsilon = 0.01$.

$$Q = ka + \frac{9}{4}bk\eta_1^2A_c^2 + \frac{3}{4}bk\eta_2^2\Omega^2A_c^2 + \frac{3}{2}bk\eta_1\eta_2\Omega A_c^2 + \alpha\Gamma_1 - \epsilon\mu \left(\Gamma_2 + \frac{3}{2}bk\eta_1\eta_2A_c^2 \right),$$

$$P = 3\mu bk\eta_1\eta_2\Omega^2A_c^2 + \alpha\mu\Gamma_2\Omega^2 - \epsilon\mu^2 \left(\frac{1}{4}\gamma_1A_c^2 - \frac{1}{8}\gamma_2A_c^4 \right.$$

$$\left. + \frac{5}{64}\gamma_3A_c^6 - \frac{7}{128}\gamma_4A_c^8 - ka - \frac{9}{4}kb\eta_1^2A_c^2 - \frac{3}{4}kb\eta_2^2\Omega^2A_c^2 - \alpha\Gamma_1 \right),$$

and the parameters containing Eq. (11) are given in Appendix C.

The resonant property of the neuron described by the theoretical (dark solid line) and numerical (dark solid line) frequency-response curves, without the coupling effects of adaption and EMI, is exhibited in Fig. 2(a). The numerically computed A_c

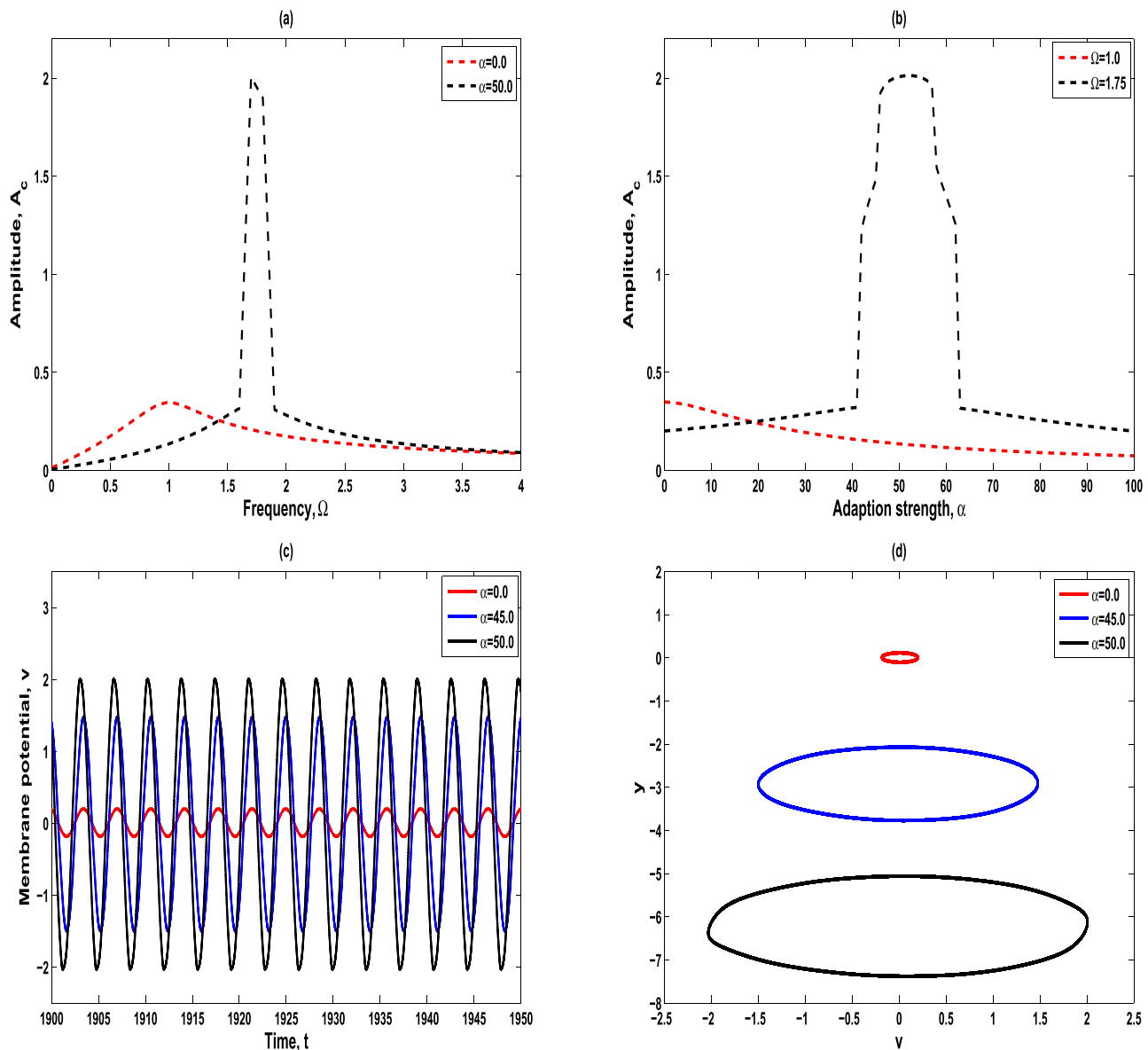


FIG. 3. Frequency-response curves for values of α (a). Curves of amplitude vs α for values of Ω (b). Time series (c) and corresponding phase portraits for values of α (d) and for $l = 0.3$ and $\Omega = 1.75$. The parameters used are as follows: $k = 0.0$, $k_1 = 0.1$, $k_2 = 0.5$, $a = 0.1$, $b = 0.06$, $r = 0.01$, $s = 4.0$, $\alpha_0 = -1.1$, $\alpha_1 = 2.7778$, $\alpha_2 = 2.3333$, $\alpha_3 = 0.7619$, $\alpha_4 = 0.0847$, $c = 100.0$, and $\epsilon = 0.01$.

is in nearly agreement with the theoretical approximation. In the absence of EMI, and for $I = 1$, $\alpha_0 = -1.1$, and $\alpha_n = 0, 50$, and 150 , the response amplitude A_c is found to be maximum at $\Omega_n = 1, 1.75$, and 2.75 , respectively [see Fig. 2(b)]. In Fig. 2(c) for $\omega_n = 0.5$ as α_n increases, A_c decreases, and resonance is not observed, the signal

is not detected. Therefore, for $\Omega_n = 1, 1.75$, and 2.75 , resonance is found at $\alpha_n = 0, 50$, and 150 , respectively, and the signal is detected. Ω_n and Ω_a are, respectively, the numerical and analytical frequencies, while α_n and α_a are, respectively, the numerical and analytical adaption strengths. The above resonance phenomenon is termed

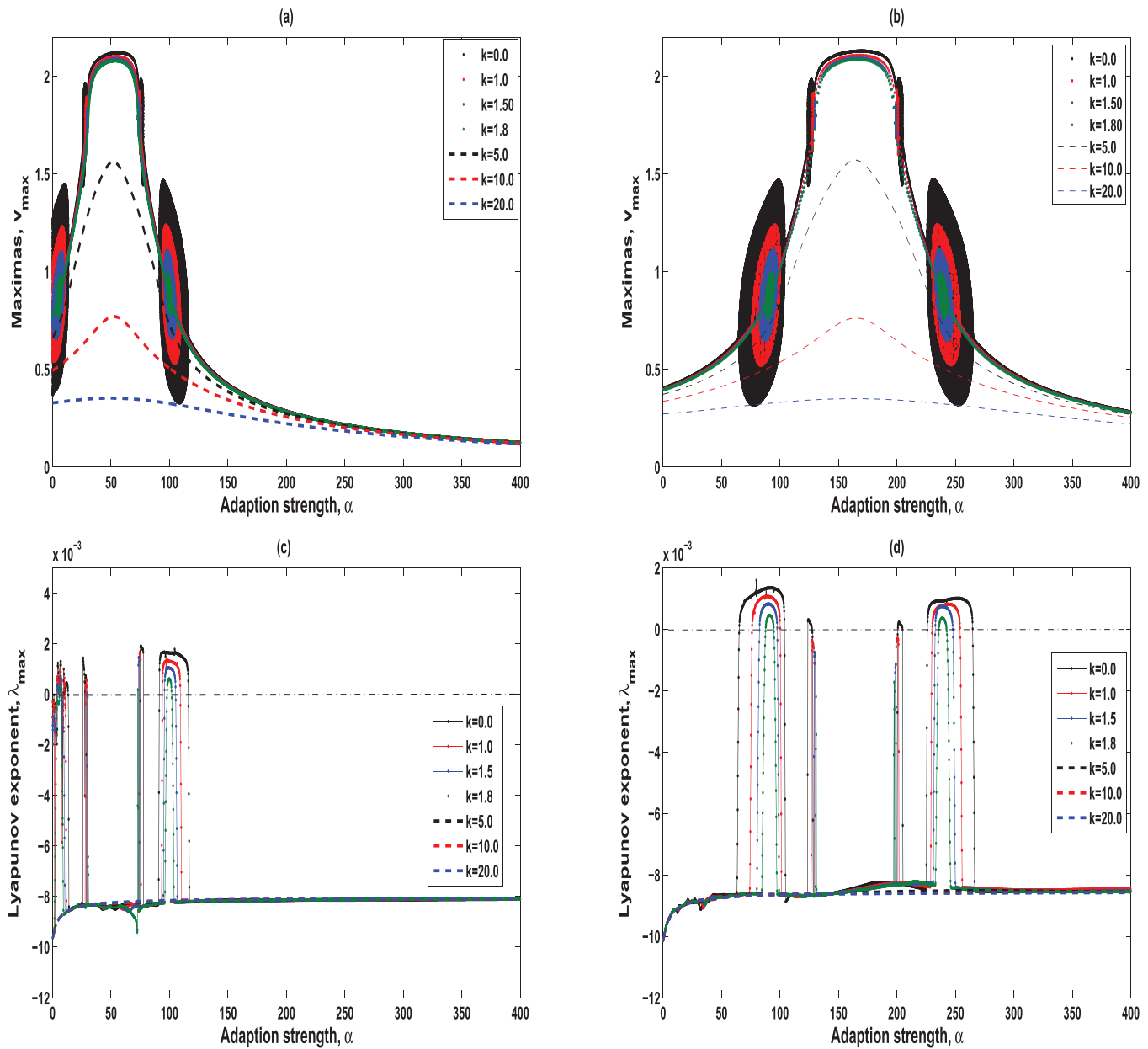


FIG. 4. Bifurcation diagrams (a) and (b) and variation in corresponding Lyapunov exponents (c) and (d) vs the coupling strength α for different values of the EMI strength k . The parameters used are as follows: $\Omega = 1.75$ (a) and (c); $\Omega = 2.75$ (b) and (d); and $I = 1.0$, $k_1 = 0.1$, $k_2 = 0.5$, $a = 0.1$, $b = 0.06$, $r = 0.01$, $s = 4.0$, $\alpha_0 = -1.1$, $\alpha_1 = 2.7778$, $\alpha_2 = 2.3333$, $\alpha_3 = 0.7619$, $\alpha_4 = 0.0847$, $c = 100.0$, and $\epsilon = 0.01$.

10 November 2023 09:35:48

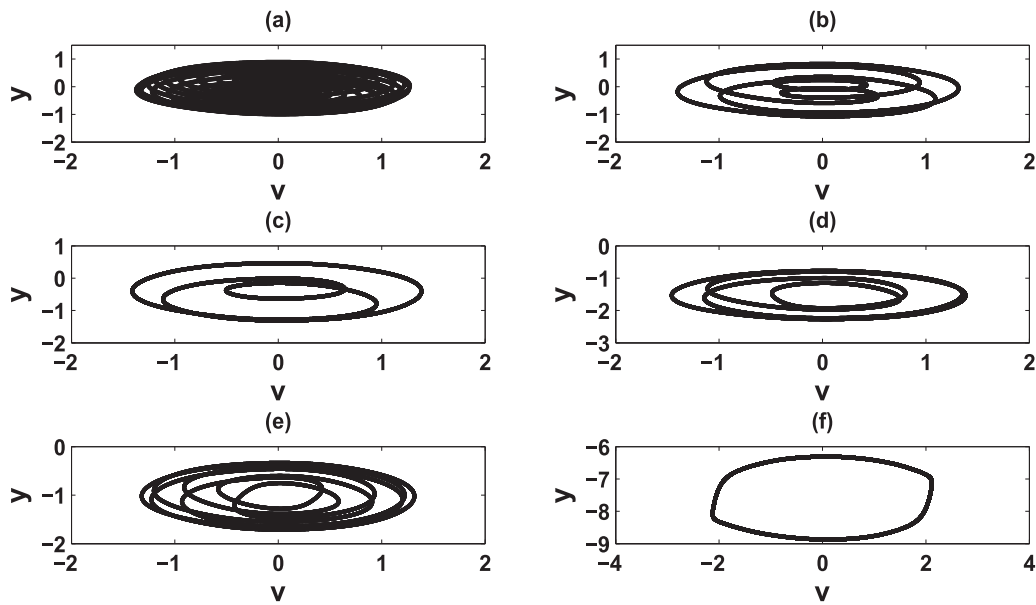


FIG. 5. Map in (v) and (y) plane of an existence of chaotic attractor (a), period-5 (b), period-3 (c), period-4 (d), period-7 (e), and period-1 (f) waves per breath for some values of α . The parameters used are as follows: $\alpha = 0.5$ (a), $\alpha = 2$ (b), $\alpha = 8.5$ (c), $\alpha = 96.6$ (d), $\alpha = 104.3$ (e), $\alpha = 50$ (f), $\Omega = 1.75$, $l = 1.0$, $k = 0.0$, $k_1 = 0.1$, $k_2 = 0.5$, $a = 0.1$, $b = 0.06$, $r = 0.01$, $s = 4.0$, $\alpha_0 = -1.1$, $\alpha_1 = 2.7778$, $\alpha_2 = 2.3333$, $\alpha_3 = 0.7619$, $\alpha_4 = 0.0847$, $c = 100.0$, and $\epsilon = 0.01$.

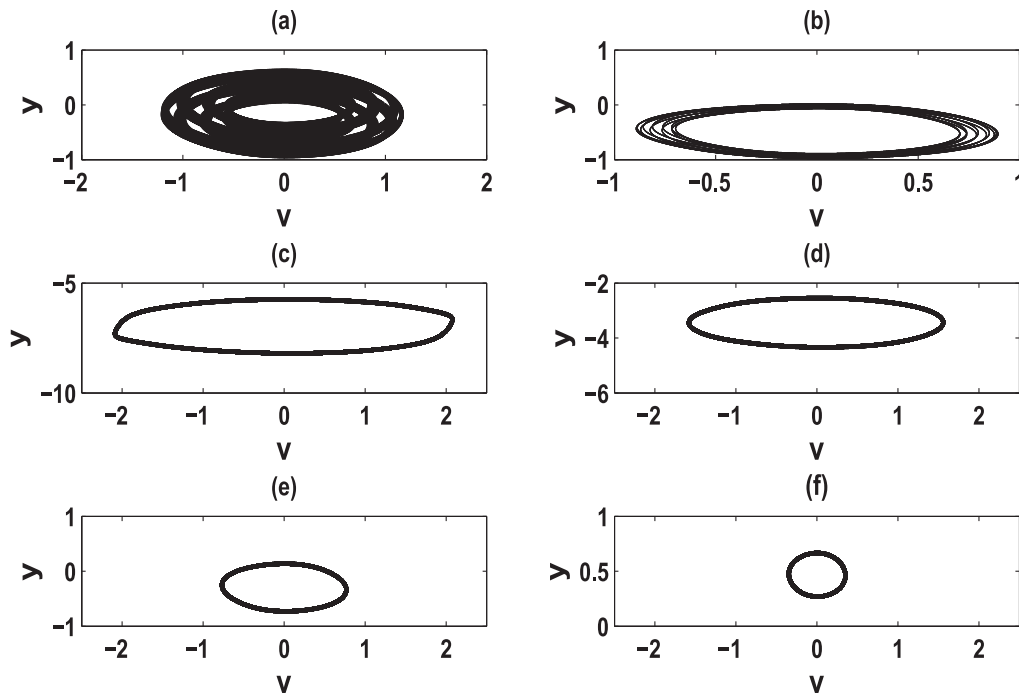


FIG. 6. Map in (v) and (y) plane of an existence of chaotic attractor (a), period-10 waves per breath (b), and period-1 wave (c)–(f) for some values of α and k . The parameters used are as follows: $\alpha = 4$, $k = 1$ (a); $\alpha = 104.7$, $k = 1.5$ (b); $\alpha = 50$: $k = 1$ (c), $k = 5$ (d), $k = 10$ (e), $k = 20$ (f); and $\Omega = 1.75$, $l = 1.0$, $k_1 = 0.1$, $k_2 = 0.5$, $a = 0.1$, $b = 0.06$, $r = 0.01$, $s = 4.0$, $\alpha_0 = -1.1$, $\alpha_1 = 2.7778$, $\alpha_2 = 2.3333$, $\alpha_3 = 0.7619$, $\alpha_4 = 0.0847$, $c = 100.0$, and $\epsilon = 0.01$.

as adaptive resonance (AR), as it is due to the presence of adaption currents. This phenomenon is like vibrational resonance, but here the resonance is not due to the presence of a high-frequency external periodic force as shown in Ref. 5–7, although the adaptation currents behave like it. Thus, signal detection in neuronal systems could be self-improved by adaption currents instead of noise (stochastic resonance).^{1–4} Furthermore, the frequency response and the dynamics of the system are also impacted by feedback k [Fig. 2(d)].

In fact, when k is small, the occurrence of AR in single neurons is found requiring less energy even if the resonant peak of the response reduces, ensuring optimal detection performance. This fact shows that the AR in this neuron with EMI is a less energy-consuming process than that without EMI. For large values of k , the resonance peak is definitely damped. k_n and k_a being, respectively, the numerical and analytical EMI strengths k . The latter reveal the characteristics necessary to trigger a nerve pulse (excitation) from

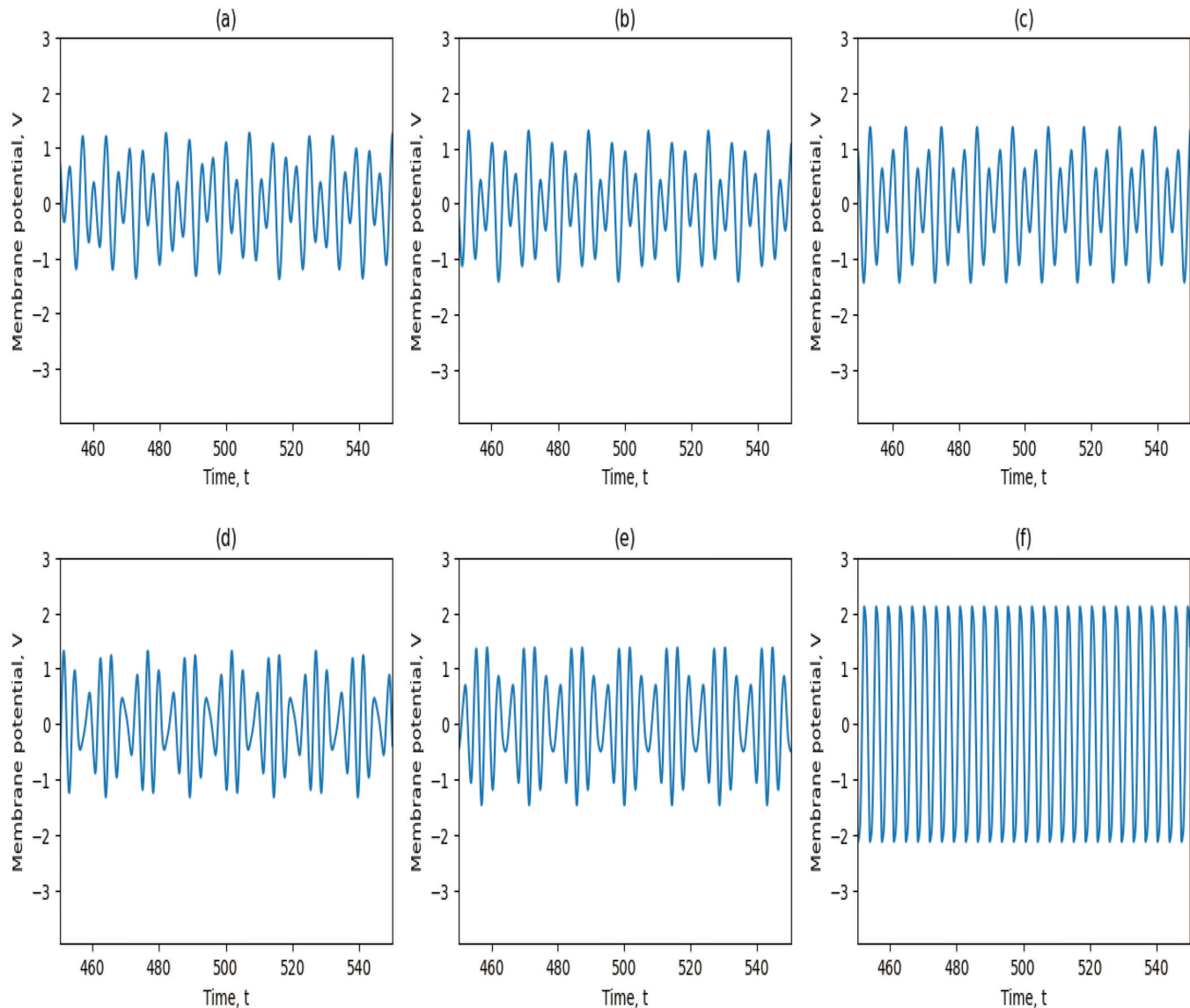


FIG. 7. Time series of different states for different values of adaption strength α without EMI. Chaotic breathing (a), period-5 (b), period-3 (c), period-7 (d), period-4 (e), and period-1 (f) wave per breath for some values of α . The parameters used are as follows: $\alpha = 0.5$ (a), $\alpha = 2$ (b), $\alpha = 8.5$ (c), $\alpha = 104.3$ (d), $\alpha = 96.6$ (e), $\alpha = 50$ (f), and $l = 1.0$, $\Omega = 1.75$, $k = 0.0$, $k_1 = 0.1$, $k_2 = 0.5$, $\alpha = 0.1$, $\beta = 0.06$, $r = 0.01$, $s = 4.0$, $\alpha_0 = -1.1$, $\alpha_1 = 2.7778$, $\alpha_2 = 2.3333$, $\alpha_3 = 0.7619$, $\alpha_4 = 0.0847$, $c = 100.0$, and $\epsilon = 0.01$.

the rest by detection through adaption currents, the optimization of energy to provide AR by a small EMI, and the recovery state by a strong EMI (inhibition) in the nerve cell.

The detection phenomenon of a small external current is shown and explained in Fig. 3. In fact, for $I = 0.3$, $\alpha_0 = -1.1$, and without adaption and EMI effects, the neuron system is in a resting state for any initial condition [see Figs. 3(a) and 3(b) red dots]. Therefore, for the same small external current with an adaption, the system can fire at a certain value of adaption strength $\alpha = 50.0$ [see Figs. 3(a) and 3(b) black dots]. The detection appears at the same value of adaption strength for $I = 0.3$ [$\alpha = 50.0$, see Fig. 3(b) black dots] and for $I = 1.0$ [$\alpha = 50.0$, see Fig. 2(c) green dots], so the intensity of the external stimulus does not change the value of α at which resonance occurs. Time series and corresponding phase portraits obtained for different values of adaption strength according to Figs. 3(a) and 3(b) are exhibited in Figs. 3(c) and 3(d). The latter explains the help of self-detection in the neuron system by the reaching of potential levels necessary to fire (generate a pulse). The neuron's capacity for self-adaption can increase its sensitivity to even minor outside effects.

The bifurcation diagrams [see Figs. 4(a) and 4(b)] and the corresponding variation in the Lyapunov exponents [see Figs. 4(c) and 4(d)] vs adaption strength α are represented to verify qualitatively the behaviors of our neuronal system evoked by the previous theoretical analysis. The asymptotic dynamics of our

system [Eq. (2)] are described in Fig. 4 when $\Omega_n = 1.75$ [see Figs. 4(a) and 4(c)] and $\Omega_n = 2.75$ [see Figs. 4(b) and 4(d)], under the effects of electromagnetic induction through some values of its strength k . In addition to adaptive resonance behavior, we found that adaptive variable creates period doubling and chaotic motion phenomena symmetrically from the resonance peak [see Figs. 4(a) and 4(b)]. In addition to the reduction or optimization of the resonance peak, the period doubling and chaotic motion are controlled and even destroyed when electromagnetic induction increases [see Figs. 4(a) and 4(b)].

The phase portraits confirm the period doubling and chaotic behaviors mentioned by the Lyapunov and bifurcation diagrams for a resonance frequency of $\Omega = 1.75$ and the zero electromagnetic flux $k = 0$ (Fig. 5). For $\alpha = 0.5$, the neuron exhibits a chaotic response [see Fig. 5(a)], and the membrane potential responses are aperiodic and irregular. The membrane potential is in the n -wave periodic packets in every stimulus period [see Figs. 5(b) and 5(f)]. In fact, we have packets behavior with $n = 5$, $n = 3$, $n = 7$, $n = 4$, and $n = 1$ waves per packet, for $\alpha = 2$ (b), $\alpha = 8.5$ (c), $\alpha = 104.3$ (d), $\alpha = 96.6$ (e), and $\alpha = 50$ (f), respectively. For non-zero and small EMI, period doubling and chaotic motion can also be found [see Figs. 6(a) and 6(b)]. For large values of EMI strength, the system admits only a periodic motion, whose amplitude decreases significantly as the strength k increases [see Figs. 6(c)–6(f)]. The latter explains the regulation of the neuron activity leading to a

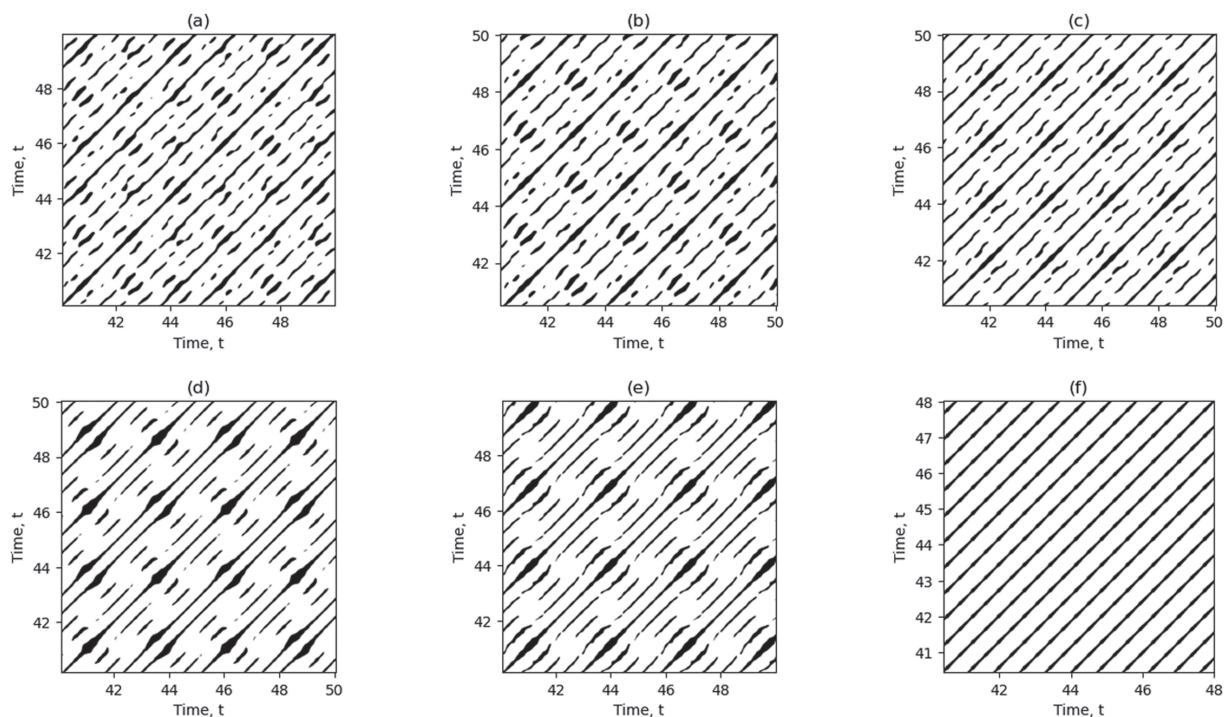


FIG. 8. RPs of the membrane potential voltage v for different values of the adaption strength α without EMI. Chaotic breathing (a), period-5 (b), period-3 (c), period-7 (d), period-4 (e), and period-1 (f) wave per breath for some values of α . The parameters used are as follows: $\alpha = 0.5$ (a), $\alpha = 2$ (b), $\alpha = 8.5$ (c), $\alpha = 104.3$ (d), $\alpha = 96.6$ (e), $\alpha = 50$ (f), and $\Omega = 1.75$, $k = 0.0$, $I = 1.0$, $k_1 = 0.1$, $k_2 = 0.5$, $\alpha_0 = 0.1$, $\beta = 0.06$, $r = 0.01$, $s = 4.0$, $\alpha_0 = -1.1$, $\alpha_1 = 2.7778$, $\alpha_2 = 2.3333$, $\alpha_3 = 0.7619$, $\alpha_4 = 0.0847$, $c = 100.0$, and $\epsilon = 0.01$. The recurrence threshold ϵ is selected to ensure a recurrence point density of 0.15.

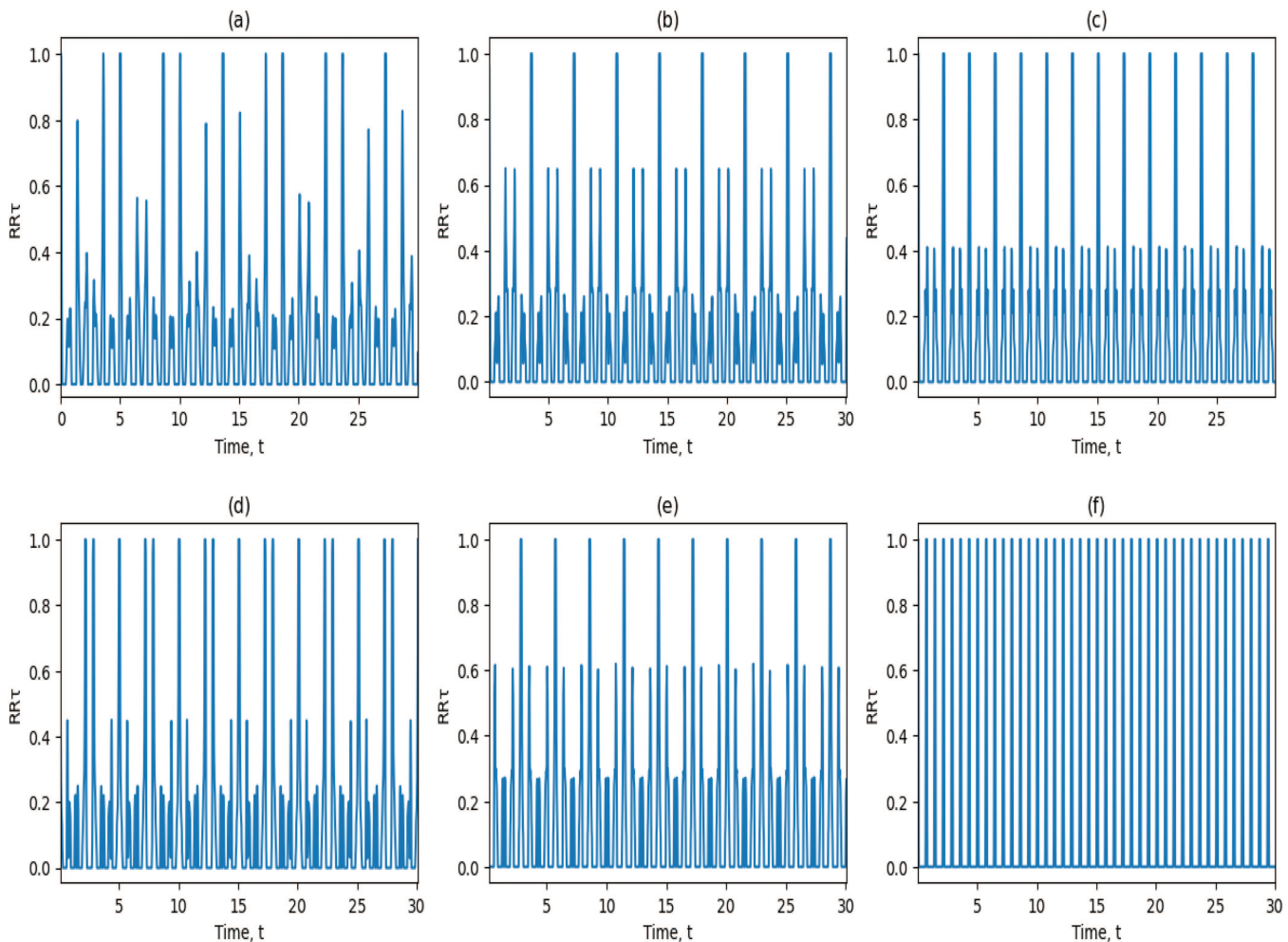


FIG. 9. Probability of recurrence after time τ (τ -recurrence rate) for the membrane potential voltage v for different values of the adaption strength α without EMI. chaotic breathing (a), period-5 (b), period-3 (c), period-7 (d), period-4 (e), and period-1 (f) wave per breath for some values of α . The parameters used are as follows: $\alpha = .5$ (a), $\alpha = 2$ (b), $\alpha = 8.5$ (c), $\alpha = 104.3$ (d), $\alpha = 96.6$ (e), $\alpha = 50$ (f) and $\Omega = 1.75, l = 1.0, k = 0.0, k_1 = 0.1, k_2 = 0.5, \alpha = 0.1, \beta = 0.06, r = 0.01, s = 4.0, \alpha_0 = -1.1, \alpha_1 = 2.7778, \alpha_2 = 2.3333, \alpha_3 = 0.7619, \alpha_4 = 0.0847, c = 100.0,$ and $\epsilon = 0.01$. The number of waves per breath is visible as the rather thin side peaks of the main peaks (in addition to the main peak).

quiescent potential constant value [see Fig. 6(f)] after an emission of an optimal action potential.

IV. RECURRENCE QUANTIFICATION ANALYSIS

We next use the recurrence plots to investigate certain recurrence features of the neuron dynamics in its corresponding phase space.^{8,9} It is a qualitative tool to detect even hidden features graphically. We define the tool that measures recurrences of a trajectory $\vec{x}(t) \in \mathbf{R}^m$ (with m being the dimension of the system) of a dynamical system. The dynamical similarity is measured in terms of some metric distance $d_{i,j} = \|\vec{x}_i - \vec{x}_j\|$ defined in the phase space. Based on the resulting distance matrix $(d_{i,j})$, we say that the trajectory has

returned at time $t = j$ to the former point in phase space visited at $t = i$, if the distance between the two associated state vectors is smaller than or equal to a threshold ϵ . The corresponding recurrence matrix has entries 1 for pairs (i, j) of close distance and 0 elsewhere,

$$R_{i,j}(\epsilon) = \Theta(\epsilon - d_{i,j}), \tag{12}$$

where Θ is the Heaviside function and $i \in [1, N]$, with N being the length of time series. The recurrence plot (RP) is the representation of this binary matrix. The threshold ϵ is selected in a way that ensures a certain recurrence point density;^{9,37} we use for this analysis $\epsilon = 0.15$. The RP of the times series represented in Fig. 7 uncover how neurons can encode their electrical activities

(Fig. 8). The dashed-dotted diagonal line in the RPs corresponds to a wave, and for the alternating wave behavior, we have a set of dashed lines followed by an extended black region (see Figs. 8). The number of waves per breath is well distinguished by the number of dashed lines. The block-like black region represents the silent state between each group of stimulus, which is the refractory period of the neuron (period for which the neuron cannot respond to a stimulus). Figures 8(b)–8(f) exhibit the type coding of periodic breathing [see Figs. 8(b)–8(e)] and spiking activities [see Fig. 8(f)], respectively. The pattern on Fig. 8(a) has a random appearance showing the encoding of a chaotic message by the neuron. Finally, the RPs in Fig. 8 explain the ways that the neuron uses to encode its behaviors and that the coding looks very different depending on adaption strength. To go beyond the visual impression of the RP, we calculate several measures of complexity that quantify small-scale structures in RPs, proposed in Ref. 9, 38 and known as the recurrence quantification analysis (RQA) based on the recurrence point density and the diagonal and vertical line structures of the RP. Our aim here is to give an estimator of the probability that the system returns to its previous state after time τ also called the τ -recurrence rate. The simplest measure of the RQA is the recurrence rate (RR) defined by $\frac{1}{M^2} \sum R_{ij}$ corresponding to the probability that a state will recur.⁹ An estimator of the probability τ -recurrence rate can be given by

$$RR_{\tau}(\varepsilon) = \frac{1}{M - \tau} \sum_{i=0}^{M-\tau} R_{i,i+\tau}(\varepsilon), \quad (13)$$

where τ is the set time and M is the total number of points in the phase space. The distance between the peaks in an RR_{τ} plot corresponds to the period length between breaths and the inter-wave intervals of wave trains. The specific probability distributions for recurrence after lag τ of the wave trains of 3 waves, 5 waves, 7 waves, 4 waves, and 1 wave reveal remarkable differences [Figs. 9(b)–9(f)]. We observe a uniform probability distribution produced by these wave trains, revealing different periodicities and large blocks between the breathing periods [see Figs. 9(b)–9(f)]. The RR_{τ} of chaotic breathing has a more complicated distribution of peaks corresponding to an unpredictable occurrence of waves [Fig. 9(a)].

V. CONCLUSION

First, in this paper, we considered an extended memristive Fitzhugh–Nagumo bursting model, taking into account adaptation and electromagnetic induction (EMI) effects. The model contains high order terms in the transmembrane function with coefficients α_1 , α_2 , α_3 , α_4 , and α_0 that play the role of maximum coefficients of ion channel conductance. In the system without adaption and EMI, monostability, bistability, and tristability were found by numerical and analytical calculations using the fourth-order Runge–Kutta algorithm and Lindstedt's perturbation method, respectively.²⁹ In the tristability zone, the system exhibits three attractors: the first is a steady state (resting state); the second is an oscillation with a smaller amplitude (subthreshold state); and the third is an oscillation with the largest amplitude (emission of the neuronal pulse). The corresponding unstable states are thresholds separating stable states. Such

multistability behavior is relevant for understanding the initiation and information processing in many neurons.

Second, we studied the simultaneous effects of adaption and EMI on the neuronal dynamic of the monostable activity (resting state). Adaptive resonance and the control of the resonance peak were found by numerical and analytical calculations using the fourth-order Runge–Kutta algorithm and the harmonic balance method³⁰ due to the presence of internal effects of adaption and EMI. Thus, adaption strength was found to enhance self-detection of weak signals while EMI was found to optimize or inhibit the membrane potential. Bifurcation diagrams and corresponding Lyapunov exponents exhibited periodic and chaotic behaviors vs adaptation strength, which were controlled and even destroyed for a weak and a strong EMI, respectively. The phase portraits and time series were drawn, showing periodic and chaotic breathing structures and spiking. The triggering of an action potential (depolarization) through adaptation and the recovery to the silent state (repolarization) through strong EMI are relevant for the understanding of information processing and regulation after activities in neurons.

Finally, the representation of the dynamics of the neurons' membrane voltages by recurrence plots⁹ provided a convenient approach to compare even the hidden recurrence features of their breathing patterns. These breathing patterns were highly varying because they were found to be very sensitive to changes in the adaption strength, explaining their relevance to adapt neurons under external influences. The richness of different breathing pattern structures can permit an enhancement to encode information, especially the chaotic pattern, whose random appearance and broad spectrum could be used to enhance the privacy of an encoded message in the communication.

An experimental illustration of the obtained results as an open research question using an electronic circuit would be interesting. It would be also important to extend the recurrence analysis using available data of the present work.

AUTHOR DECLARATIONS

Conflict of Interest

The authors have no conflicts to disclose.

Author Contributions

I. B. Tagne Nkonga: Conceptualization (lead); Data curation (lead); Formal analysis (lead); Investigation (lead); Methodology (lead); Software (lead); Validation (lead); Writing – original draft (lead); Writing – review & editing (lead). **N. Marwan:** Supervision (equal); Validation (equal). **F. M. Moukam Kakmeni:** Supervision (equal). **R. Yamapi:** Supervision (equal). **Jürgen Kurths:** Supervision (equal).

DATA AVAILABILITY

The data that support the findings of this study are available from the corresponding author upon reasonable request.

APPENDIX A: THE DETERMINISTIC MODEL (2)

The classical FHN model has the form

$$\begin{aligned} \frac{dv}{dt} &= f(v) - w + I, \\ \frac{dw}{dt} &= av - bw, \end{aligned} \tag{A1}$$

where $f(v)$ is a polynomial of the third degree and a and b are constant parameters. The model allows a geometrical explanation of neuronal excitability and mechanisms for spike generation.³⁹ It can explain the absence of all-or-none spikes, excitation block, spike accommodation, and other effects.⁴⁰

We propose the following extended system:

$$\begin{aligned} \frac{dv}{dt} &= \alpha_0 v + \alpha_1 v^3 - \alpha_2 v^5 + \alpha_3 v^7 - \alpha_4 v^9 + \alpha y + I, \\ \frac{dy}{dt} &= \epsilon(\beta - cv - dv^2 - ey), \end{aligned} \tag{A2}$$

where higher-order terms are additionally included as $f(v) = \alpha_0 v + \alpha_1 v^3 - \alpha_2 v^5 + \alpha_3 v^7 - \alpha_4 v^9$ as well as an additional term dv^2 in the equation for the recovery variable y . Only odd terms are kept in $f(v)$ to keep odd symmetry of the function as in the original FHN model.

The extension (A2) can also be motivated by the ML model,

$$\frac{dv}{dt} = I(t) + \frac{1}{C} [g_{Ca} m_\infty(v)(v_{Ca} - v) + g_K w(v_K - v) + g_L(v_L - v)], \tag{A3a}$$

$$\frac{dw}{dt} = \frac{w_\infty(v) - w}{\tau_w(v)}, \tag{A3b}$$

with

$$m_\infty(v) = \frac{1}{2} + \frac{1}{2} \tanh\left(\frac{v - v_1}{v_2}\right), \tag{A4a}$$

$$w_\infty(v) = \frac{1}{2} + \frac{1}{2} \tanh\left(\frac{v - v_3}{v_4}\right), \tag{A4b}$$

$$\tau_w(v) = \frac{T_0}{\cosh\left(\frac{v - v_3}{2v_4}\right)}. \tag{A4c}$$

System (A3a)–(A3b) consists of the voltage-gated C_a^{2+} current, the delayed rectified K^+ current, and the leak current, respectively. The membrane potential of the neuron and the activation variable of K^+ ion channels are represented by variables v and w , respectively. The maximum conductance functions of C_a^{2+} , K^+ , and the leak currents are described by parameters g_{Ca} , g_K , and g_L , respectively.

Furthermore, v_{Ca} , v_K , and v_L stand for the reversal potentials of different ionic current functions while $I(t)$ is the applied stimulus current. C is the membrane capacitance, and it is considered unity. T_0 is the temperature scaling factor of the K^+ channel opening, while v_1 , v_2 , v_3 , and v_4 represent the other scaling parameters of the model.²⁸

Equation (A2) can be treated as a truncated Taylor expansion of (A3a)–(A3b) around the zero point. However, since some terms of the expansion, such as even or mixed terms in the voltage equation, are omitted, this is not a rigorous expansion but rather serves as an analogy,

$$\begin{aligned} \alpha_0 &= -\frac{151v_1^8}{2688v_2^9}g_{Ca}v_{Ca} - \frac{17v_1^6}{90v_2^7}g_{Ca}v_{Ca} + \frac{v_1^4}{3v_2^5}g_{Ca}v_{Ca} - \frac{v_1^2}{2v_2^3}g_{Ca}v_{Ca} \\ &\quad + \frac{1}{2v_2}g_{Ca}v_{Ca} - \frac{151v_1^9}{24192v_2^9}g_{Ca} - \frac{17v_1^7}{630v_2^7}g_{Ca} + \frac{v_1^5}{15v_2^5}g_{Ca} \\ &\quad - \frac{v_1^3}{6v_2^3}g_{Ca} + \frac{v_1}{2v_2}g_{Ca} - \frac{1}{2}g_{Ca} - g_L, \\ \alpha_1 &= -\frac{151v_1^7}{672v_2^9}g_{Ca} + \frac{17v_1^5}{30v_2^7}g_{Ca} + \frac{2v_1^3}{3v_2^5}g_{Ca} - \frac{v_1}{2v_2^3}g_{Ca} - \frac{151v_1^6}{288v_2^9}g_{Ca}v_{Ca} \\ &\quad - \frac{17v_1^4}{18v_2^7}g_{Ca}v_{Ca} - \frac{151v_1^6}{288v_2^9}g_{Ca}v_{Ca} - \frac{17v_1^4}{18v_2^7}g_{Ca}v_{Ca} \\ &\quad + \frac{2v_1^2}{3v_2^5}g_{Ca}v_{Ca} - \frac{1}{6v_2^3}g_{Ca}v_{Ca}, \\ \alpha_2 &= -\frac{151v_1^5}{192v_2^9}g_{Ca} - \frac{17v_1^3}{18v_2^7}g_{Ca} + \frac{v_1}{3v_2^5}g_{Ca} - \frac{151v_1^4}{192v_2^9}g_{Ca}v_{Ca} \\ &\quad - \frac{17v_1^2}{30v_2^7}g_{Ca}v_{Ca} + \frac{1}{15v_2^5}g_{Ca}v_{Ca}, \\ \alpha_3 &= -\frac{151v_1^3}{288v_2^9}g_{Ca} - \frac{17v_1}{90v_2^7}g_{Ca} - \frac{151v_1^2}{672v_2^9}g_{Ca}v_{Ca} - \frac{17}{630v_2^7}g_{Ca}v_{Ca}, \\ \alpha_4 &= -\frac{151v_1}{288v_2^9}g_{Ca} - \frac{151}{24192v_2^9}g_{Ca}v_{Ca}, \\ \beta &= -g_K v_K, \\ \alpha &= \frac{v_3^2}{48v_4^4} + \frac{5v_3^3}{48v_4^4} - \frac{11v_3^5}{720v_4^4} + \frac{47v_3^6}{7560v_4^4} + \frac{17v_3^9}{15120v_4^4}, \\ c &= \frac{1}{6v_4} - \frac{v_3}{24v_4^2} - \frac{5v_3^2}{16v_4^3} + \frac{11v_3^4}{144v_4^5} - \frac{47v_3^6}{1080v_4^7} - \frac{17v_3^8}{1680v_4^9}, \\ d &= \frac{1}{48v_4^2} + \frac{5v_3}{16v_4^3} - \frac{11v_3^3}{72v_4^5} + \frac{329v_3^5}{2520v_4^7} + \frac{204v_3^7}{5040v_4^9}, \\ e &= -\frac{v_3^2}{24v_4^2} - \frac{1}{3}. \end{aligned}$$

The above constants can be estimated if we refer to the parameters of the ML neuronal model defined in Ref. 28; for example, with $C = 1$, $g_L = 0.5$, $v_L = -0.5$, $g_{Ca} = 1.2$, $v_{Ca} = 1$, $g_K = 2$, $v_K = -0.7$, $v_1 = -0.01$, $v_2 = 0.15$, $v_3 = 0.1$, $v_4 = 0.05$, and $T_0 = 3$, we can say that these constants will be of the order: $0 < \alpha_0 \leq 2.85$; $0 < \alpha_1 \leq 236$; $0 < \alpha_2 \leq 989$; $0 < \alpha_3 \leq 1.76 \times 10^4$; $0 < \alpha_4$

$\leq 3.1173 \times 10^4$; $0 < \beta \leq 1.4$; $0 < c \leq -106.5$; $0 < d \leq 3.5129 \times 10^3$; $0 < e \leq -0.5$; and $0 \leq \alpha \leq 2.95$.

APPENDIX B: THE COEFFICIENTS OF EQUATION (4)

We apply the Lindsted's perturbation method²⁹ with the Ansatz,

$$v(\tau) = v_0(\tau) + \mu v_1(\tau) + \mu^2 v_2(\tau) + \dots, \tag{B1}$$

where $v_n(\tau)$ ($n = 0, 1, 2, \dots$) are 2π -periodic functions. Moreover, $\tau = \omega t'$, where the frequency ω can be represented by the expansion

$$\omega = \omega_0 + \mu \omega_1 + \mu^2 \omega_2 + \dots, \tag{B2}$$

with ω_n ($n = 0, 1, 2, \dots$) constants determined in Eq. (6).

By substituting Eqs. (B1) and (B2) in Eq. (3) and finding secular terms for the different order of the parameter μ , a solution to Eq. (3) can be approximated by Eq. (4), with

$$\begin{aligned} \theta_2 &= \frac{79}{1280} \gamma_4 A^9 - \frac{73}{1024} \gamma_3 A^7 + \frac{\gamma_2}{12} A^5 - \frac{3}{32} A^3, \\ \theta_3 &= -\frac{1}{32} \left(\frac{7}{16} \gamma_4 A^9 - \frac{9}{16} \gamma_2 A^7 + \frac{3}{4} \gamma_2 A^5 - \gamma_1 A^3 \right), \\ \theta_4 &= -\frac{1}{384} \left(\frac{5}{4} \gamma_4 A^9 - \frac{5}{4} \gamma_3 A^7 + \gamma_2 A^5 \right), \\ \theta_5 &= -\frac{1}{3072} \left(\frac{7}{4} \gamma_4 A^9 - \gamma_3 A^7 \right), \quad \theta_6 = -\frac{1}{20480} \gamma_4 A^9. \end{aligned}$$

APPENDIX C: THE COEFFICIENTS OF EQUATION (11)

$$\begin{aligned} F_1 &= \frac{49}{16384} \gamma_4^2 + \frac{49}{16384} \frac{\epsilon^2 \mu^2 \gamma_4^2}{\Omega^2}, \\ F_2 &= -\frac{35}{4096} \gamma_3 \gamma_4 - \frac{35}{4096} \frac{\epsilon^2 \mu^2 \gamma_3 \gamma_4}{\Omega^2}, \\ F_3 &= \frac{7}{512} \gamma_2 \gamma_4 + \frac{25}{4096} \gamma_3^2 + \frac{7}{512} \frac{\epsilon^2 \mu^4 \gamma_2 \gamma_4 + \frac{25}{4096} \epsilon^2 \mu^4 \gamma_3^2}{\mu^2 \Omega^2}, \\ F_4 &= \frac{7}{64} \left(-\frac{1}{4} \gamma_1 + \frac{9}{4} b k \eta_1^2 + \frac{3}{4} b k \Omega^2 \eta_2^2 + \frac{3}{2} b k \eta_1 \eta_2 (-\epsilon \mu + \Omega) \right) \gamma_4 - \frac{5}{256} \gamma_2 \gamma_3 \\ &\quad + \frac{7}{64} \frac{\left(3 \mu b k \eta_1 \eta_2 \Omega^2 - \frac{1}{4} \epsilon \mu^2 \gamma_1 + \frac{9}{4} \epsilon \mu^2 b k \eta_1^2 + \frac{3}{4} \epsilon \mu^2 b k \eta_2^2 \right) \epsilon \mu^2 \gamma_4 - \frac{5}{256} \epsilon^2 \mu^4 \gamma_2 \gamma_3}{\mu^2 \Omega^2}, \\ F_5 &= -\frac{5}{32} \left(-\frac{1}{4} \gamma_1 + \frac{9}{4} b k \eta_1^2 + \frac{3}{4} b k \Omega^2 \eta_2^2 + \frac{3}{2} b k \eta_1 \eta_2 (-\epsilon \mu + \Omega) \right) \gamma_3 + \frac{1}{64} \gamma_2^2 \\ &\quad + \frac{7}{64} \frac{\left(-\alpha \epsilon \mu \Gamma_2 + a k + \alpha \Gamma_1 + \gamma_0 \right) \gamma_4 + \frac{7}{64} \left(\alpha \mu \Gamma_2 \Omega^2 - \Omega^2 + 1 + \epsilon \mu^2 (a k + \alpha \Gamma_1) \right) \epsilon \mu^2 \gamma_4}{\mu^2 \Omega^2} \\ &\quad - \frac{5}{32} \frac{\left(3 \mu b k \eta_1 \eta_2 \Omega^2 - \frac{1}{4} \epsilon \mu^2 \gamma_1 + \frac{9}{4} \epsilon \mu^2 b k \eta_1^2 + \frac{3}{4} \epsilon \mu^2 b k \eta_2^2 \right) \epsilon \mu^2 \gamma_3 + \frac{1}{64} \epsilon^2 \mu^4 \gamma_2^2}{\mu^2 \Omega^2}, \\ F_6 &= -\frac{5}{32} \left(-\alpha \epsilon \mu \Gamma_2 + a k + \alpha \Gamma_1 + \gamma_0 \right) \gamma_3 + \frac{1}{4} \gamma_2 \left(-\frac{1}{4} \gamma_1 + \frac{9}{4} b k \eta_1^2 + \frac{3}{4} b k \Omega^2 \eta_2^2 + \frac{3}{2} b k \eta_1 \eta_2 (-\epsilon \mu + \Omega) \right) \\ &\quad + \frac{1}{4} \frac{\left(3 \mu b k \eta_1 \eta_2 \Omega^2 - \frac{1}{4} \epsilon \mu^2 \gamma_1 + \frac{9}{4} \epsilon \mu^2 b k \eta_1^2 + \frac{3}{4} \epsilon \mu^2 b k \eta_2^2 \right) \epsilon \mu^2 \gamma_2 - \frac{5}{32} \left(\alpha \mu \Gamma_2 \Omega^2 - \Omega^2 + 1 + \epsilon \mu^2 (a k + \alpha \Gamma_1) \right) \epsilon \mu^2 \gamma_3}{\mu^2 \Omega^2}, \end{aligned}$$

10 November 2023 09:35:48

$$\begin{aligned}
 F_7 &= \frac{1}{4}\gamma_2(-\alpha\epsilon\mu\Gamma_2 + ak + \alpha\Gamma_1 + \gamma_0) + \left(-\frac{1}{4}\gamma_1 + \frac{9}{4}bk\eta_1^2 + \frac{3}{4}bk\Omega^2\eta_2^2 + \frac{3}{2}bk\eta_1\eta_2(-\epsilon\mu + \Omega)\right)^2 \\
 &+ \frac{\left(3\mu bk\eta_1\eta_2\Omega^2 - \frac{1}{4}\epsilon\mu^2\gamma_1 + \frac{9}{4}\epsilon\mu^2bk\eta_1^2 + \frac{3}{4}\epsilon\mu^2bk\eta_2^2\right)^2}{\mu^2\Omega^2} + \frac{1}{4}\frac{\left(\alpha\mu\Gamma_2\Omega^2 - \Omega^2 + 1 + \epsilon\mu^2(ak + \alpha\Gamma_1)\right)\epsilon\mu^2\gamma_2}{\mu^2\Omega^2}, \\
 F_8 &= 2\left(-\alpha\epsilon\mu\Gamma_2 + ak + \alpha\Gamma_1 + \gamma_0\right)\left(-\frac{1}{4}\gamma_1 + \frac{9}{4}bk\eta_1^2 + \frac{3}{4}bk\Omega^2\eta_2^2 + \frac{3}{2}bk\eta_1\eta_2(-\epsilon\mu + \Omega)\right) \\
 &+ \frac{2\left(\alpha\mu\Gamma_2\Omega^2 - \Omega^2 + 1 + \epsilon\mu^2(ak + \alpha\Gamma_1)\right)\left(3\mu bk\eta_1\eta_2\Omega^2 - \frac{1}{4}\epsilon\mu^2\gamma_1 + \frac{9}{4}\epsilon\mu^2bk\eta_1^2 + \frac{3}{4}\epsilon\mu^2bk\eta_2^2\right)}{\mu^2\Omega^2}, \\
 F_9 &= \left(-\alpha\epsilon\mu\Gamma_2 + ak + \alpha\Gamma_1 + \gamma_0\right)^2 + \frac{\left(\alpha\mu\Gamma_2\Omega^2 - \Omega^2 + 1 + \epsilon\mu^2(ak + \alpha\Gamma_1)\right)^2}{\mu^2\Omega^2}.
 \end{aligned}$$

REFERENCES

- ¹B. McNamara and K. Wiesenfeld, *Phys. Rev. A* **39**, 4854 (1989).
- ²B. McNamara, K. Wiesenfeld, and R. Roy, *Phys. Rev. Lett.* **60**, 2626 (1988).
- ³L. Gammaitoni, P. Hänggi, P. Jung, and F. Marchesoni, *Rev. Mod. Phys.* **70**(1), 223 (1998).
- ⁴T. Kanamaru, T. Horita, and Y. Okabe, "Stochastic resonance in Hodgkin-Huxley network," *J. Phys. Soc. Jpn.* **67**, 4058–4063 (1998).
- ⁵V. Baysal and E. Yilmaz, "Effects of electromagnetic induction on vibrational resonance in single neurons and neuronal networks," *Physica A* **537**, 122733 (2020).
- ⁶P. S. Landa and P. V. McClintock, *J. Phys. A: Math. Gen.* **33**, L433 (2000).
- ⁷S. Jeyakumari, V. Chinnathambi, S. Rajasekar, and M. A. Sanjuan, "Single and multiple vibrational resonance in a quintic oscillator with monostable potentials," *Phys. Rev. E* **80**, 046608 (2009).
- ⁸J. P. Eckmann, S. Oliffson Kamphorst, and D. Ruelle, "Recurrence plots of dynamical systems," *Europhys. Lett.* **4**, 973–977 (1987).
- ⁹N. Marwan, M. C. Romano, M. Thiel, and J. Kurths, "Recurrence plots for the analysis of complex systems," *Phys. Rep.* **438**, 237–329 (2007).
- ¹⁰I. B. Tagne Nkouna, N. Marwan, R. Yamapi, and J. Kurths, "Recurrence-based analysis and controlling switching between synchronous silence and bursting states of coupled generalized FitzHugh-Nagumo models driven by an external sinusoidal current," *Nonlinear Dyn.* (submitted).
- ¹¹A. M. Nkomidjo, E. K. Ngamga, B. R. N. Nbenjo, J. Kurths, and N. Marwan, "Recurrence-based synchronization analysis of weakly coupled bursting neurons under external ELF fields," *Entropy* **24**, 235 (2022).
- ¹²P. Faure and H. Korn, "A nonrandom dynamic component in the synaptic noise of a central neuron," *Proc. Natl. Acad. Sci. U. S. A.* **94**(12), 6506–6511 (1997).
- ¹³H. Hoang, E. J. Lang, Y. Hirata, I. T. Tokuda, K. Aihara, K. Toyama, M. Kawato, and N. Schweighofer, "Electrical coupling controls dimensionality and chaotic firing of inferior olive neurons," *PLoS Comput. Biol.* **16**(7), e1008075 (2020).
- ¹⁴I. B. Tagne Nkouna, L. Messee Goulefack, R. Yamapi, and J. Kurths, "Switching from active to non-active states in a conductance-based neuronal model under electromagnetic induction," *Nonlinear Dyn.* **111**, 771–788 (2022).
- ¹⁵L. M. Goulefack, A. C. Chamgoue, C. Anteneodo, and R. Yamapi, "Stability analysis of the Hindmarsh–Rose neuron under electromagnetic induction," *Nonlinear Dyn.* **108**, 2627–2642 (2022).
- ¹⁶A. S. Tankou Tagne, C. N. Takembo, H. G. Ben-Bolie, and P. Owona Ateba, "Localized nonlinear excitations in diffusive memristor-based neuronal networks," *PLoS One* **14**(6), e0214989 (2019).
- ¹⁷A. S. Etémé, C. B. Tabi, and A. Mohamadou, "Firing and synchronization modes in neural network under magnetic stimulation," *Commun. Nonlinear Sci. Numer. Simul.* **72**, 432–440 (2019).
- ¹⁸C. B. Tabi, A. S. Etémé, A. Mohamadou, and T. C. Kofané, "Unstable discrete modes in Hindmarsh–Rose neural networks under magnetic flow effect," *Chaos, Solitons Fractals* **123**, 116–123 (2019).
- ¹⁹F. Zhan and S. Liu, *Front. Comput. Neurosci.* **11**, 107 (2017).
- ²⁰J. Ma, F. Wu, and C. Wang, *Int. J. Modern Phys. B* **31**(2), 1650251 (2017).
- ²¹Y. Zhang, F. Wu, C. Wang, and J. Ma, *Physica A* **521**, 519–530 (2019).
- ²²J. L. Hindmarsh and R. M. Rose, "A model of neuronal bursting using three coupled first-order differential equations," *Proc. R. Soc. London B* **221**(1222), 87–102 (1984).
- ²³I. B. Tagne Nkouna, F. M. Moukam Kakmeni, B. I. Camara, and R. Yamapi, "Controlling switching between birhythmic states in a new conductance-based bursting neuronal model," *Nonlinear Dyn.* **107**(10), 2887–2902 (2022).
- ²⁴I. B. Tagne Nkouna, Y. Xia, S. Yanchuk, R. Yamapi, and J. Kurths, "Generalized FitzHugh–Nagumo model with tristable dynamics: Deterministic and stochastic bifurcations," *Chaos, Solitons Fractals* **175**, 114020 (2023).
- ²⁵J. L. Hindmarsh and R. M. Rose, "A model of the nerve impulse using two first-order differential equations," *Nature* **296**, 162–164 (1982).
- ²⁶R. FitzHugh, "Impulses and physiological states in theoretical model of nerve membrane," *Biophys. J.* **1**, 445–466 (1961).
- ²⁷A. L. Hodgkin and A. F. Huxley, "A quantitative description of membrane current and its application to conduction and excitation in nerve," *J. Physiol.* **117**, 500–544 (1952).
- ²⁸C. Moris and H. Lecar, "Voltage oscillations in the barnacle giant muscle fiber," *Biophys. J.* **35**(1), 193–213 (1981).
- ²⁹P. Hagedorn, *Non-Linear Oscillations*, 2nd ed. (Clarendon Press, Oxford, 1988).
- ³⁰A. H. Nayfeh and D. T. Mook, *Nonlinear Oscillations* (John Wiley & Sons, New York, 1979).
- ³¹M. Lv, C. N. Wang, G. D. Ren, J. Ma, and X. L. Song, "Model of electrical activity in a neuron under magnetic flow effect," *Nonlinear Dyn.* **85**, 1479–1490 (2016).
- ³²Q. D. Li, H. Z. Zeng, and J. Li, "Hyperchaos in a 4D memristive circuit with infinitely many stable equilibria," *Nonlinear Dyn.* **79**, 2295–2308 (2015).
- ³³F. Parasteh, K. Rajagopal, A. Karthikeyan, A. Alsaedi, T. Hayat, and V. T. Pham, "Complex dynamics of a neuron model with discontinuous magnetic induction and exposed to external radiation," *Cogn. Neurodyn.* **12**, 607–614 (2018).
- ³⁴N. G. Lloyd, "Lienard systems with several limit cycles," *Math. Proc. Camb. Phil. Soc.* **102**, 565 (1987).
- ³⁵H. Fukai, S. Doi, T. Nomura, and S. Sato, "Hopf bifurcations in mutipleparameter space of the Hodgkin–Huxley equations I. Global organization of bistable periodic solutions," *Biol Cybern.* **82**(3), 215 (2000).
- ³⁶E. M. Izhikevich, *Dynamical Systems in Neuroscience: The Geometry of Excitability and Bursting* (MIT Press, 2006).

³⁷K. H. Kraemer, R. V. Donner, J. Heitzig, and N. Marwan, "Recurrence threshold selection for obtaining robust recurrence characteristics in different embedding dimensions," *Chaos* **28**(8), 085720 (2018).

³⁸J. P. Zbilut and C. L. Webber, Jr., "Embeddings and delays as derived from quantification of recurrence plots," *Phys. Lett. A* **171**, 199–203 (1992).

³⁹E. M. Izhikevich and R. FitzHugh, "FitzHugh-Nagumo model," *Scholarpedia* **1**(9), 1349 (2006).

⁴⁰I. B. Tagne Nkouna, F. M. Moukam Kakmeni, and R. Yamapi, "Birhythmic oscillations and global stability analysis of a conductance-based neuronal model under channel fluctuations," *Chaos, Solitons Fractals* **159**, 112126 (2022).